GMR
The Original

STRUCTURAL AND DYNAMIC CHARACTERIZATION OF SOFO INTERACTION WITH SARS-COV-2 RDRP–RNA COMPLEX USING MOLECULAR DYNAMICS SIMULATIONS

Sameer Ojha[1], Muralidhar[1], Rakesh Kumar Tiwari[1*]

[1]Department of physics, Deen Dayal Upadhyay Gorakhpur University Gorakhpur India,
***Corresponding Author**: Rakesh Kumar Tiwari, drrkt@yahoo.com

ABSTRACT
Computational biophysics has emerged as a powerful strategy for drug discovery and mechanistic investigation of biomolecular systems. The global epidemic of corona virus disease 2019 (COVID-19), caused by severe acute respiratory syndrome corona virus 2, has highlighted the urgent need for effective antiviral therapeutics. Viral replication of SARS COVID-19 is mediated by the RNA dependent RNA polymerase (RdRp), a key enzyme responsible for viral genome synthesis and a validated target of the antiviral drug Sofosbuvir Di-phosphate (Sofo). In this study, we performed molecular dynamics (MD) simulations using the AMBER-18 package to investigate the binding behavior and structural influence of Sofo on the SARS-COVID-19 RdRp complex in the presence of double-stranded RNA to show how, the RNA residue interact to bind the Sofo and provide the stability of the complex. Structural stability and interaction profiles were evaluated through analyses of root-mean-square deviation (RMSD), root-mean-square fluctuation (RMSF), radius of gyration (Rg), and hydrogen bonding patterns. Further, the binding free energy '-39.4 kcal/mol' shows that Sofo is much suitable for RdRp non-structural protein as inhibitors.
The simulation results indicate stable binding of the ligand within the RdRp active site, accompanied by conformational modulation of the enzyme RNA complex. These findings suggest that the compound effectively interferes with RdRp function, thereby inhibiting viral RNA replication. Overall, this study provides molecular-level insights into the mechanism of RdRp inhibition and offers a rational base for the design of antiviral agents targeting SARS-CoV-2 replication.

KEYWORDS: RdRp, COVID-19, RMSD, RMSF, Hydrogen bond interactions

INTRODUCTION

Computational chemistry has become an essential tool in modern drug discovery and biomolecular analysis [1-4]. The COVID-19 pandemic, caused by SARS-CoV-2, has necessitated the identification of effective antiviral targets [5-7]. Among these, RNA-dependent RNA polymerase (RdRp) plays a vital role in viral RNA replication [7-10]. RdRp catalyzes RNA synthesis and contains conserved motifs critical for enzymatic activity [11, 12]. Due to its absence in human cells, it is considered an ideal therapeutic target [13-17]. Sofosbuvir Di-phosphate, a nucleotide analog, has shown promising antiviral activity by inhibiting RdRp function [18, 19]. However, detailed molecular-level insights into its interaction with the RdRp RNA complex remain crucial [20-23].
This research show that how, the RNA residue interacts to bind the Sofo and provide the stability of the complex in the presence of double stranded RNA.

Computational Details

The initial structure of the RdRp RNA complex was obtained from the Protein Data Bank (PDB ID: 4WTG) [24, 25]. Missing residues and atoms were modeled prior by using xleap to Molecular Dynamics (MD) simulations as shown in figure 1 while drug Sofo named as 6GS (2′-fluoro, 2′-C-methyl uridine analogue and a di-phosphate) binds in this complex shown in (figure 2). The system was parameterized using the ff99SB force field for proteins and bsc1 parameters for RNA, while the TIP3P model was used for water molecules. Potassium ions were added to neutralize the system [25, 26].



Figure 1: 3-D structure of RdRp enzyme with different motifs.

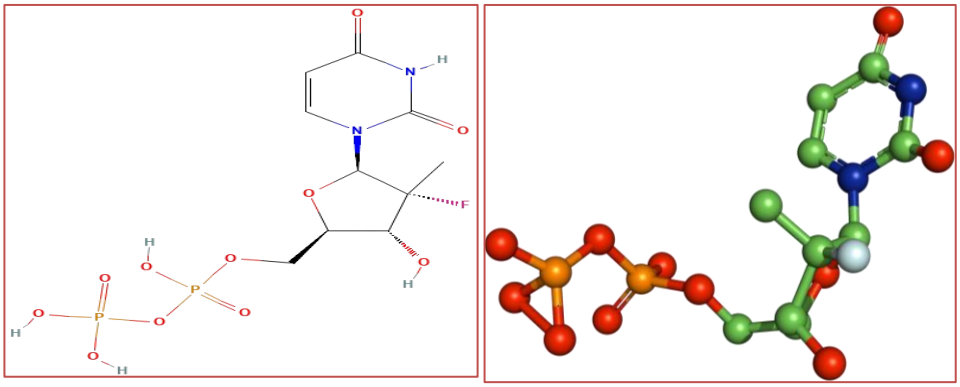


Figure 2: 2-D and 3-D structure of Sofo.

Ligand charges were calculated using the RESP method based on quantum chemical calculations [27-29]. Molecular dynamics simulations were carried out using the AMBER-18 software package under periodic boundary conditions of 12.0 Å to analyze structural dynamics [30]. The entire initial steps of MD simulations are according to previous RdRp paper of our MD simulations Lab [31, 33]. All the parameters have been generated using CPPTRAJ of AMBER package [34-39].

RESULTS AND DISCUSSION

Structural Stability Analysis

The RMSD results indicate that the system reaches equilibrium during the simulation period, demonstrating overall stability of the RdRp RNA Sofo complex. The ligand exhibits minimal deviation, suggesting strong binding affinity within the active site. The RMSD plot of the complex, as shown in figure 4, shows that, the enzyme is stable at 2.0 Å, the RNA at 1.9 Å, and the drug, as named Sofo, is stable at less than 0.8 Å, indicating good convergence during simulation. The orientations of complex at different simulations time shown in figure 5.

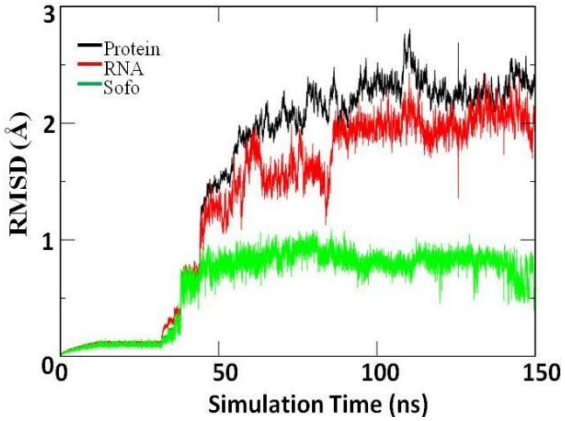


Figure 4: The root mean square deviations (RMSD) plot of the complex as a function of simulations time.

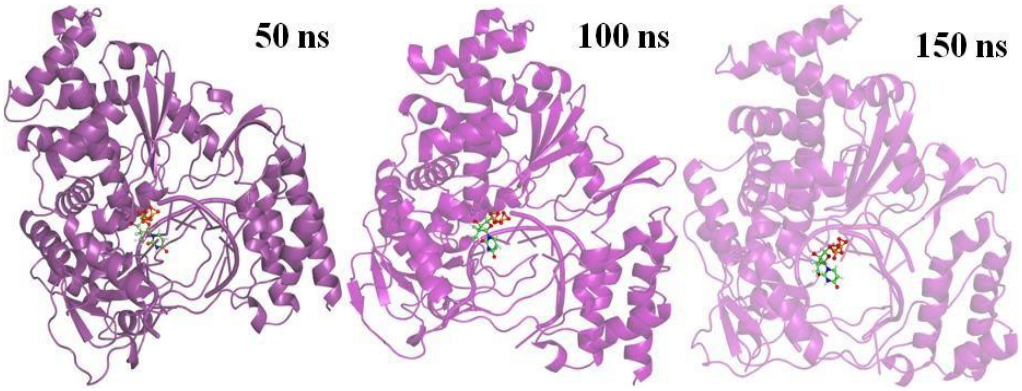


Figure 5: Snapshots of complex orientations at different times during the simulation.

Residue Flexibility

Root Mean Square Fluctuations (RMSF) analysis reveals localized flexibility in loop regions and active site residues, which is essential for accommodating ligand binding and RNA movement. Figure 6 shows the RMSF plot of the complex, in this plot the atoms lie in the RdRp shows much stability for the requirements of binding the drugs.

Further for the stability, the radius of gyration of the Sofo ligand has been analyzed using the formula given in equation (1) [38-40].

$$R_g = \sqrt{\frac{\sum_{i=1}^{n}(m_i)(x_i - x_{cm})^2}{\sum_{i=1}^{n} m_i}} \qquad (1)$$

Where mi denotes the mass of ith particle, xi is the position vector of ith and xcm denote the center of mass. Figure 7 shows variations of radius of gyration of the complex taken during simulation time, representing the structure is overall stable during the simulations time at
25.3 Å.

Overall stability parameters such as RMSD, RMSF and radius of gyration (Rg) providing the information about the good binding role of Sofo for RdRp non-structural protein.

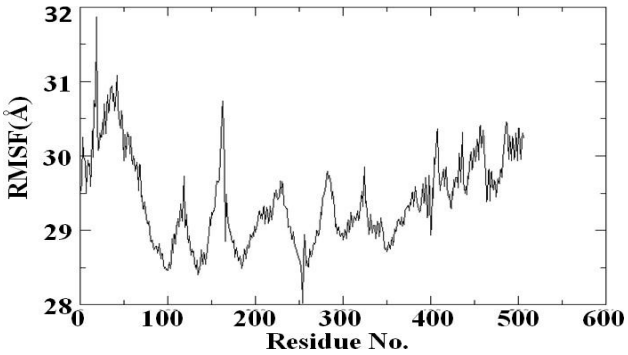


Figure 6: Root Mean Square Fluctuations vs. Atom No. plot.

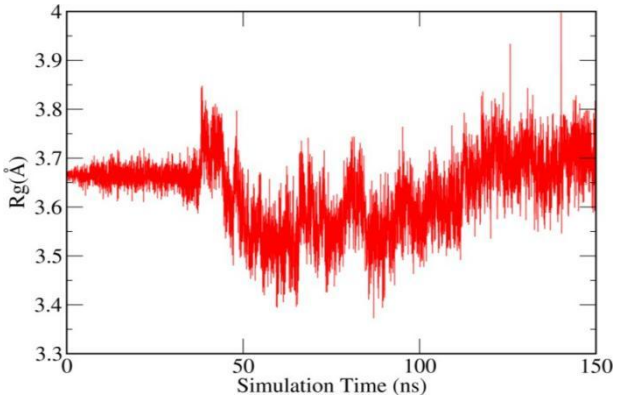


Figure 7: The Radius of gyration plot as a function of simulation time

Hydrogen Bonding Interactions

Hydrogen bond analysis confirms the formation of stable interactions between Sofo and surrounding residues. Notably, Lys409 and U515 play a significant role in maintaining ligand stability through stable hydrogen bonding. Figure 8 shows the hydrogen bond interactions of Sofo to its RNA as well as enzymes residues. From the plot, the hydrogen bond interactions of Sofo with enzymes residue LYS409 and uracile (U515) are much stronger and stable during the whole simulations. The hydrogen bond interactions with the enzyme and RNA residues shown in figure 9.

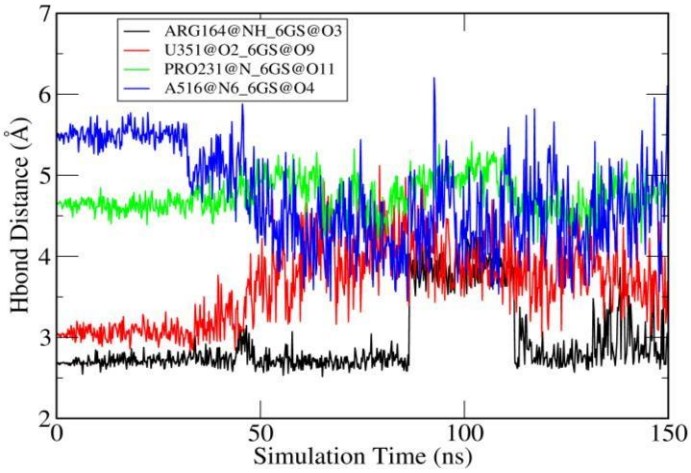


Figure 8: Hydrogen bond interactions plot as functions of simulations time.

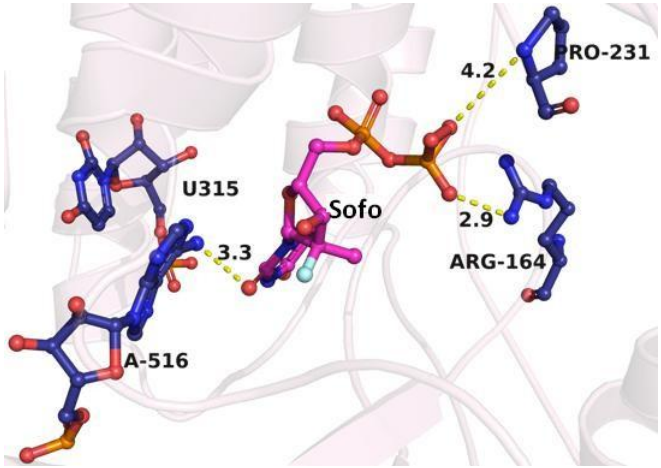


Figure 9: The snapshot of hydrogen bond interaction taken during trajectory analysis.

The interaction between Lys409 and U515 functions as a dynamic regulatory element, influencing RNA conformational changes and contributing to the overall stability of the complex. These interactions are essential for understanding the inhibitory mechanism of Sofo.

3.4. MM/GBSA Binding free energy calculation

For more binding affinity of Sofo in RdRp non-structural protein, the binding free energy has been calculated using MM/GBSA (Molecular Mechanics/Generalized Born Surface Area).

The binding for last 100 frame of stable trajectory have been calculated. The MM/GBSA energy of the complex is found to be '-47680.9 kcal/mol' where as the energy of receptor and Sofo (drugs) are '-45432.3 kcal/mol' and '-2209.2 kcal/mol' respectively, providing the total binding free energy '-39.4 kcal/mol'. This B.E result shows that Sofo is much suitable for RdRp non-structural protein as inhibitors.

Further, the residue-wise MM/GBSA energy decomposition was performed to identify the amino-acid residues that make the major energetic contributions to the binding of Sofo within the protein binding site. As shown in Figure 10, all of the analyzed residues exhibit negative total decomposition energies, indicating that they contribute favorably to the overall protein–ligand association. However, the magnitude and energetic origin of these contributions vary considerably among the individual residues, suggesting that Sofo recognition is governed by a combination of electrostatic, van der Waals, and solvation effects rather than by a single dominant interaction. Among all residues Arg-447 shows the positive contribution, with a total energy of about –19.4 kcal mol^{-1}. This means Arg-447 is the strongest energetic contributor in the part studied. The large positive contribution of Arg-

447 comes mainly from electrostatic interactions. That is logical because Arg-447 has a charged guanidinium group while the phosphate part of Sofo is highly polar and negatively charged. The di-phosphate part gives a surface for electrostatic contact allowing Arg-447 to form strong Coulombic

contacts with other positively charged residues in the binding area. Arg-447 is clearly the player, in this interaction.

Arg-469 also contributes substantially to ligand stabilization, with a total contribution of approximately −12.3 kcal mol^{-1}. Its energetic profile similarly reflects a strong electrostatic component, accompanied by favorable nonpolar/van der Waals contributions. The involvement of multiple Arginine residues is particularly significant because the di-phosphate group of Sofo possesses a high density of negative charge. Consequently, the positively charged guanidinium groups can provide electrostatic anchoring and help maintain the ligand in a productive orientation within the active-site region.

A further favorable contribution is observed for Arg-417, which contributes approximately −11.5 kcal mol^{-1} to the binding free energy. The substantial contribution from Arg-417, together with those of Arg-447 and Arg-469, suggests that a cluster of positively charged residues forms an important electrostatic component of the Sofo recognition site. Such cooperative stabilization is expected to be especially important for a di-phosphorylated nucleotide analogue, for which charge complementarily strongly influences binding affinity and positional stability.

The remaining residues make moderate but consistently favorable contributions. Cys-424 contributes approximately −4.6 kcal mol^{-1}, while the other entry shown in the decomposition profile also exhibits a favorable contribution of approximately −4.5 kcal mol^{-1}. Leu-369 contributes about −5.5 kcal mol^{-1}, indicating that hydrophobic and dispersion interactions also participate in ligand stabilization. The contributions of Leu-155 and Asn-154, approximately −3.3 kcal mol^{-1} and −4.0 kcal mol^{-1} respectively, are comparatively smaller but remain favorable. Lys-204 contributes approximately −3.3 kcal mol^{-1}, whereas Lys-156 exhibits a substantially stronger contribution of approximately −11.8 kcal mol^{-1}, emphasizing that positively charged lysine residues can also contribute importantly to recognition of the di-phosphate containing ligand.

The component-wise decomposition further demonstrates that the favorable residue contributions are not derived exclusively from electrostatics. Although the electrostatic term is particularly important for the Arginine and lysine residues, it is partially opposed by the polar solvation contribution, as expected for a highly charged ligand. This energetic compensation is a characteristic feature of MM/GBSA calculations involving phosphate-containing ligands: strong direct electrostatic attraction between the ligand and protein is accompanied by an energetic penalty associated with de-solvation of polar/charged groups. Nevertheless, the resulting total decomposition energies remain negative for all residues shown in the profile, indicating that the favorable direct protein–ligand interactions outweigh the corresponding solvation penalties.

The decomposition profile therefore suggests that Sofo binding is primarily driven by electrostatic recognition of its di-phosphate group, reinforced by van der Waals and local nonpolar interactions with neighboring residues. In particular the strong contributions of Arg-447, Arg-469, Arg-417 and Lys-156 show that these residues are important parts of the binding environment. The simultaneous participation of positively charged residues may create a complementary electrostatic network around the di-phosphate group. This network helps keep the ligand in place. Holds its orientation during the molecular dynamics run. The moderate contributions from Leu-369, Leu-155, Asn-154 and Cys-424 further suggest that the binding site is kept stable by a mix of short-range interactions not just by one residue–ligand contact.

Overall the per residue decomposition analysis shows that Sofo recognition is spread over residues. Charged residues act as the main stabilizers for binding. The negative total decomposition energies, for all analyzed residues confirm that these residues participate favorably in the complex. They give energetic evidence that the binding stays stable during the molecular dynamics simulation.

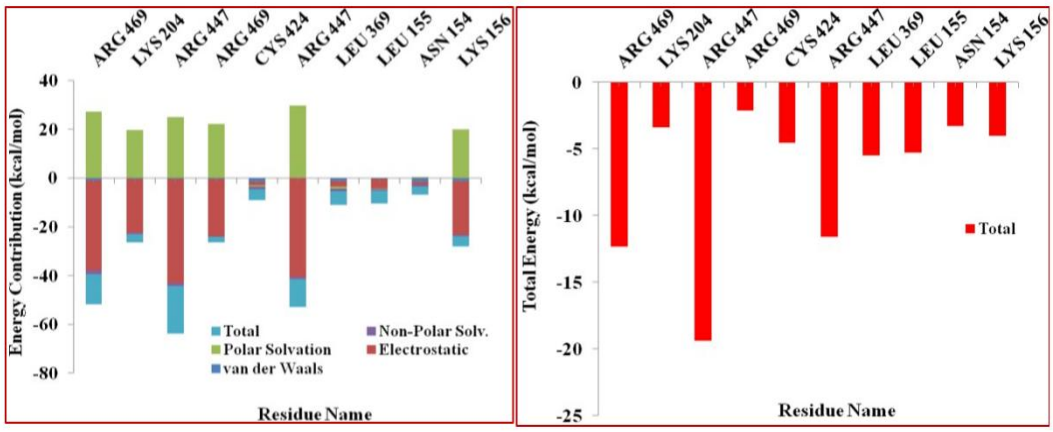


Figure 10: The energy contribution per residue (in left) and total energy per residues (in right)

CONCLUSION

The Computational molecular dynamics simulations study of SARS-CoV-2 RdRp RNA complex demonstrate the drug binding role of RdRp enzymes. This study provides detailed insights into the interaction of Sofo with the SARS-CoV-2 RdRp RNA complex. The RMSD plot of the complex shows that the enzyme and RNA are stable at 2.0 Å and
1.9 Å respectively while the Sofo drug is stable below the 0.8 Å shows its stability during the trajectory. Further, the results highlight the importance of hydrogen bonding and key residues in stabilizing ligand binding with binding energy '-39.4 kcal/mol'. These findings contribute to a deeper understanding of antiviral mechanisms and support future drug design efforts targeting RdRp.
Overall conclusions from the calculations and finding, it is obvious the uracile of the RNA residue provide much stability by the hydrogen interactions of enzyme residues.

REFERENCES

[1].Yang, L.; Liu, S.; Liu, J.; Zhang, Z.; Wan, X.; Huang, B.; Chen, Y.; Zhang, Y. COVID-19: Immunopathogenesis and immunotherapeutics. Signal Transduction and Targeted Therapy 2020, 5, 128. https://doi.org/10.1038/s41392-020-00243-2

[2].Ciotti, M.; Ciccozzi, M.; Terrinoni, A.; Jiang, W.-C.; Wang, C.-B.; Bernardini, S. The COVID-19 pandemic. Crit. Rev. Food Sci. Nutr. 2020, 60, 365–388. https://doi.org/10.1080/10408363.2020.1783198

[3].Zhu, N. et al. A Novel Coronavirus from patients with Pneumonia in China, 2019. N. Engl. J. Med. 382, 727–733 (2020).

[4].Huang, C. et al. Clinical features of patients infected with 2019 novel coronavirus in Wuhan, China. Lancet 395, 497–506 (2020).

[5]. Chen, N. et al. Epidemiological and clinical characteristics of 99 cases of 2019 novel coronavirus pneumonia in Wuhan, China: a descriptive study. Lancet 395, 507–513 (2020).

[6].Wang, D. et al. Clinical characteristics of 138 hospitalized patients with 2019 Novel Coronavirus-infected Pneumonia in Wuhan, China. JAMA. 323, 1061–1069 (2020).

[7]. Li, T. et al. Significant changes of peripheral T lymphocyte subsets in patients with severe acute respiratory syndrome. J. Infect. Dis. 189, 648–651 (2004).

[8].Cui, W. et al. Expression of lymphocytes and lymphocyte subsets in patients with severe acute respiratory syndrome. Clin. Infect. Dis. 37, 857–859 (2003).

[9].Cimini, E. et al. Different features of Vdelta2 T and NK cells in fatal and non-fatal human Ebola infections. PLoS Negl. Trop. Dis. 11, e0005645 (2017).

[10]. Reynard, S. et al. Immune parameters and outcomes during Ebola virus disease. JCI Insight. 4, e125106 (2019). 9. Liu, Y. et al. Clinical features and progression of acute respiratory distress syndrome in coronavirus disease 2019. Preprint at https://www.medrxiv.org/content/ 10.1101/2020.02.17.20024166v3 (2020).

[11]. Lippi, G. & Plebani, M. Laboratory abnormalities in patients with COVID-2019 infection. Clin. Chem Lab. Med. 58, 1131–1134 (2020).

[12]. Xu, Z. et al. Pathological findings of COVID-19 associated with acute respiratory distress syndrome. Lancet Respir. Med. 8, 420–422 (2020).

[13]. Qin, C. et al. Dysregulation of immune response in patients with COVID-19 in Wuhan, China. Clin Infect Dis. ciaa248, https://doi.org/10.1093/cid/ciaa248 (2020).

[14]. Tan, M. et al. Immunopathological characteristics of coronavirus disease 2019 cases in Guangzhou, China. Immunology 160, 261–268 (2020)

[15]. W. Yin et al., Science 2020, 368, 1499–1504.

[16]. D. G. Ahn et al., Arch. Virol. 2012, 157, 2095–2104.

[17]. R. N. Kirchdoerfer, A. B. Ward, Nat. Commun. 2019, 10, 2342.

[18]. Y. Zhai et al., Nat. Struct. Mol. Biol. 2005, 12, 980–986.

[19]. Liu, Y.; Gayle, A. A.; Wilder-Smith, A.; Rocklöv, J. The reproductive number of COVID-19 is higher compared to SARS coronavirus. J. Travel Med. 2020, 27 (2), taaa021. https://doi.org/10.1093/jtm/taaa021

[20]. Shen M, Peng Z, Xiao Y, Zhang L. Modelling the epidemic trend of the 2019 novel coronavirus outbreak in China. bioRxiv 2020. doi: https://doi.org/10.1101/2020.01.23.916726.

[21]. Liu T, Hu J, Kang M et al. Transmission dynamics of 2019 novel coronavirus (2019-nCoV). bioRxiv 2020. doi: https://doi.org/ 10.1101/2020.01.25.919787.

[22]. Read JM, Bridgen JRE, Cummings DAT, Ho A, Jewell CP. Novel coronavirus 2019-nCoV: early estimation of epidemiological parameters and epidemic predictions. medRxiv 2020. doi: https://doi.org/10.1101/2020.01.23.20018549.

[23]. Majumder, M, Mandl, KD. (2020) Early transmissibility assessment of a novel coronavirus in Wuhan, China. https://papers.ssrn.com/ abstract=3524675 (27 January 2020, date last accessed).

[24]. Appleby, T. C., Perry, J. K., Murakami, E., Barauskas, O., Feng, J., Cho, A., Fox, D., III, Wetmore, D. R., McGrath, M. E., & Edwards, T. E. (2015). Structural basis for RNA replication by the hepatitis C virus polymerase. Science, 347(6223), 771–775. https://doi.org/10.1126/science.1259210

[25]. Y. Zhai, F. Sun, X. Li, H. Pang, X. Xu, M. Bartlam, Z. Rao, Insights into SARS-CoV transcription and replication from the structure of the nsp7-nsp8 hexadecamer. Nat. Struct. Mol. Biol. 12, 980–986 (2005).

[26]. Muralidhar, K.; Tiwari, R. K. Dynamic Insights into DNA Conformational Changes and the Impact of Magnesium Ions on Topoisomerase IA Enzymes: A Molecular Dynamics Simulation Study. Int. J. Multidiscip. Res. 2024, 6 (2), Article 1234. https://doi.org/10.36948/ijfmr.2024.v06i01.13091
[27]. Murali Dhar, Rakesh Kumar Tiwari. "Molecular Dynamics Simulation Insights into Hydrogen Bonding-Mediated Conformational Changes in Topoisomerase-IB." Macromolecular Symposia, First published: 17 October 2024. https://doi.org/10.1002/masy.202400036
[28]. Tiwari, R. K., Pandey, V., Ojha, R. P., Pandey, V., & Pandey, M. (2024). Adenosyl derivatives as potential inhibitors of NS3 protease of Japanese encephalitis virus (JEV): In silico molecular insight into therapeutic discovery. Computational and Theoretical Chemistry, 114848. https://doi.org/10.1016/j.comptc.2024.114848
[29]. Vandana, K., Tiwari, R.K., Muralidhar. In Silico Study of Triethylenetetramine Binding to Human Tetraplex DNA: Insights into Anticancer Activity. Biomedical Materials & Devices (2025). https://doi.org/10.1007/s44174-025-00512-0
[30]. Vandana, K. M., Muralidhar, & Tiwari, R. K. (2024). Structural and Energetic Characterization of Perylene Di-imide Derivatives Binding to h-Tel G-quadruplex DNA. Asian Journal of Biological Research, 27(4S). https://doi.org/10.53555/AJBR.v27i4S.8307
[31]. Muralidhar, Tiwari, R. K., Mishra, V. K., Vandana, K. M., & Pandey, V. (2026). The change in Gibbs free energy regulates Topoisomerase-IB activity: A molecular dynamics and MM/GBSA study. Journal of Biomolecular Structure and Dynamics. https://doi.org/10.1080/07391102.2026.2622489
[32]. Muralidhar; Tiwari, R. K.; Mishra, V. K.; Vandana, K.; Pandey, V. The Phosphorylated Tyrosine as a Gatekeeper for Topoisomerase Catalytic Activity: A Molecular Dynamics Simulation Study. https://doi.org/10.3389/fctls.2026.1665232
[33]. Muralidhar; Mishra, V.; Tiwari, R. K. Decoding the Antibacterial Action of Bis-Benzimidazole Derivatives through Docking and Molecular Dynamics Simulations on DNA-Topoisomerase-IA. https://doi.org/10.1002/masy.70322
[34]. Mishra, V.; Muralidhar; Tiwari, R. K. A Comparative Study of Perylene Di-imide and Triethylee Tetramine with c-KIT Quadruplex DNA. https://doi.org/10.1002/masy.70324
[35]. Muralidhar, M.; Tiwari, R. K.; Mishra, V.; Mishra, V. K. Molecular Dynamics Simulations and Binding Energy Calculations Reveal the Role of Magnesium Ion in the Stability of DNA Topoisomerase-IA Enzyme in Presence of Covalent Intermediate Bond. Comput. Theor. Chem. 2025, 1286, 115454. https://doi.org/10.1016/j.comptc.2025.115454
[36]. Tiwari RK Pandey V Srivastava H Srivastava AK Mishra VK (2023) Docking and MM study of non-structural protein (NS5) of Japanese encephalitis virus with adenosyl derivatives. Front Chem https://doi.org/10.3389/fchem.2023.1258764
[37]. Yadav, S.; Kardam, V.; Tripathi, A.; TG, S.; Dubey, K. D. The Performance of Different Water Models on the Structure and Function of Cytochrome P450 Enzymes. J. Chem. Inf. Model.2022, 62 (24), 6679–6690 https://doi.org/10.1021/acs.jcim.2c00505
[38]. Bagewadi, Z. K., Khan, T. M. Y., Gangadharappa, B., et al. (2023). Molecular dynamics and simulation analysis against superoxide dismutase (SOD) target of Micrococcus luteus with secondary metabolites from Bacillus licheniformis recognized by genome mining approach. Saudi Journal of Biological Sciences, 30(3), 103753. https://doi.org/10.1016/j.sjbs.2023.103753
[39]. Rampogu, S., Lee, G., Park, J. S., Lee, K. W., & Kim, M. O. (2022). Molecular docking and molecular dynamics simulations discover curcumin analogue as a
plausible dual inhibitor for SARS-CoV-2. International Journal of Molecular Sciences, 23(3), 1771. https://doi.org/10.3390/ijms23031771
[40]. Valle Garay, A., Socas, L. B. P., Canet, L., et al. (2018). Self-homodimerization of an actinoporin by disulfide bridging reveals implications for their structure and pore formation. Scientific Reports, 8, 6614. https://doi.org/10.1038/s41598-018-
24688-2